AIAA JOURNAL
Vol. 46, No. 7, July 2008

Quiet-Flow Ludwieg Tube for Hypersonic Transition Research

Thomas J. Juliano* and Steven P. Schneider†
Purdue University, West Lafayette, Indiana 47907-1282
Selin Aradag‡
TOBB University of Economics and Technology, 06560 Ankara, Turkey
and
Doyle Knight§
Rutgers—The State University of New Jersey, Piscataway, New Jersey 08854-8058

DOI: 10.2514/1.34640

Nearly all hypersonic tunnels have turbulent nozzle-wall boundary layers that radiate acoustic noise, generating high freestream noise levels that are an order of magnitude above flight levels. A new Mach-6 quiet tunnel has been developed to provide quiet flow at high Reynolds number with low noise levels, comparable with flight. Laminar nozzle-wall boundary layers and the resulting quiet flow have now been achieved to high Reynolds numbers of 3.5×10^6/ft (11×10^6/m), after five years of shakedown. The Mach-6 quiet tunnel is the first operational hypersonic quiet tunnel with low operating costs and good optical access.

Introduction

THE understanding of laminar–turbulent transition in hypersonic boundary layers is important for prediction and control of heat transfer, skin friction, and other boundary-layer properties. Vehicles that spend extended periods at hypersonic speeds may be critically affected by the uncertainties in transition prediction, depending on their Reynolds numbers. Although slender vehicles are the primary concern, blunt vehicles are also affected by transition [1]. However, the mechanisms leading to transition are still poorly understood, even in low-noise environments.

Many transition experiments have been carried out in conventional ground-testing facilities over the past 50 years [2]. However, these experiments are contaminated by the high levels of noise that radiate from the turbulent boundary layers normally present on the wind-tunnel walls [3]. Noise level is defined here as the root-mean-square pitot pressure $\tilde{p}$ divided by mean pitot pressure $\bar{p}$. These noise levels, typically 0.5–1%, are an order of magnitude larger than those observed in flight [4,5]. These high noise levels can cause transition to occur an order of magnitude earlier than in flight [3,5]. In addition, the mechanisms of transition that are operational in small-disturbance environments can be changed or bypassed altogether in high-noise environments; these changes in the mechanisms change the parametric trends in transition [4].

Only in the last two decades have low-noise supersonic wind tunnels been developed [3,6]. This development has been difficult, because the test-section wall boundary layers must be kept laminar to avoid high levels of eddy–Mach–wave acoustic radiation from the normally present turbulent boundary layers. A Mach-3.5 tunnel was the first to be successfully developed at NASA Langley Research Center [7]. Langley then developed a Mach-6 quiet nozzle, which was used as a starting point for the new Purdue University nozzle [8]. It was removed from service due to operational conflicts and changing research priorities. The facility is now housed at Texas A&M University. The joint Boeing and U.S. Air Force Office of Scientific Research (AFOSR) Mach-6 Quiet Tunnel (BAM6QT) is the first operational hypersonic quiet tunnel with low operating costs and good optical access [9].

Received 17 September 2007; revision received 14 December 2007; accepted for publication 21 December 2007.

*Research Assistant, School of Aeronautics and Astronautics. Student Member AIAA.
†Professor, School of Aeronautics and Astronautics. Associate Fellow AIAA.
‡Assistant Professor. Member AIAA.
§Professor, Department of Mechanical and Aerospace Engineering. Associate Fellow AIAA.

Development of the Boeing/AFOSR Mach-6 Quiet Tunnel

Facility Description and Design History

Design of the BAM6QT began in 1996. From the outset, the tunnel had two goals: run with a low noise level and do so affordably. The target was to achieve quiet flow for stagnation pressures up to 150 psia (1000 kPa). This corresponds to a unit Reynolds number of 3.4×10^6/ft. (11×10^6/m) for a stagnation temperature of 433 K at Mach 6. Quiet facilities require low levels of noise in the inviscid flow entering the nozzle through the throat, and they require laminar boundary layers on the nozzle walls [10,11]. Many of the characteristics of the NASA Langley Research Center (LaRC) quiet tunnels were employed. For example, the BAM6QT incorporates boundary-layer suction before the throat, and the nozzle features a long straight-walled section to delay the onset of Görtler vortices [12]. The first 0.76 m of the nozzle features an electroformed nickel finish, which has no seams and can be highly polished with minimal roughness and waviness [13].

To have a low operating cost, a Ludwieg tube design was chosen over the blowdown configuration (Fig. 1). A Ludwieg tube is a pipe with a converging/diverging nozzle on the end. The Ludwieg tube is operated through many cycles of expansion-wave reflection within the driver, providing a run time of a few seconds, during which the Reynolds number falls quasi-statically. Modern instrumentation makes this moderately short run time more than sufficient for measurements of instability and transition. Compared with a blowdown tunnel, the run-time and air-supply costs are reduced by one or two orders of magnitude. The complex and costly settling chamber is eliminated, and the necessary high-quality air filtering is carried out during the slow charging of the driver tube, which is maintained as a clean room. For the BAM6QT, the run time is about 7 or 8 s, whereas the tunnels at LaRC typically ran for up to 60 min and could run continuously [3].

Figure 2 shows section 8, the last nozzle section. The region of useful quiet flow lies between the characteristics marking the onset of uniform flow and the characteristics marking the upstream boundary of acoustic radiation from the onset of turbulence in the nozzle-wall boundary layer. A 7.5-deg sharp cone is drawn on the figure. The rectangles are drawn on the nozzle at the location of window

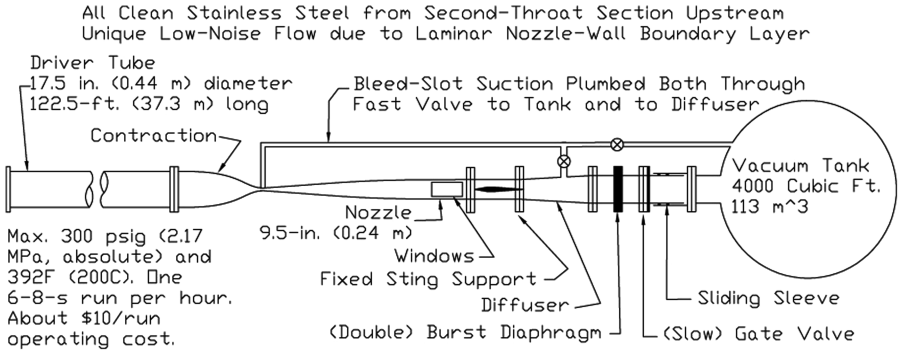

Fig. 1 Schematic of the Boeing/AFOSR Mach-6 Quiet Tunnel.

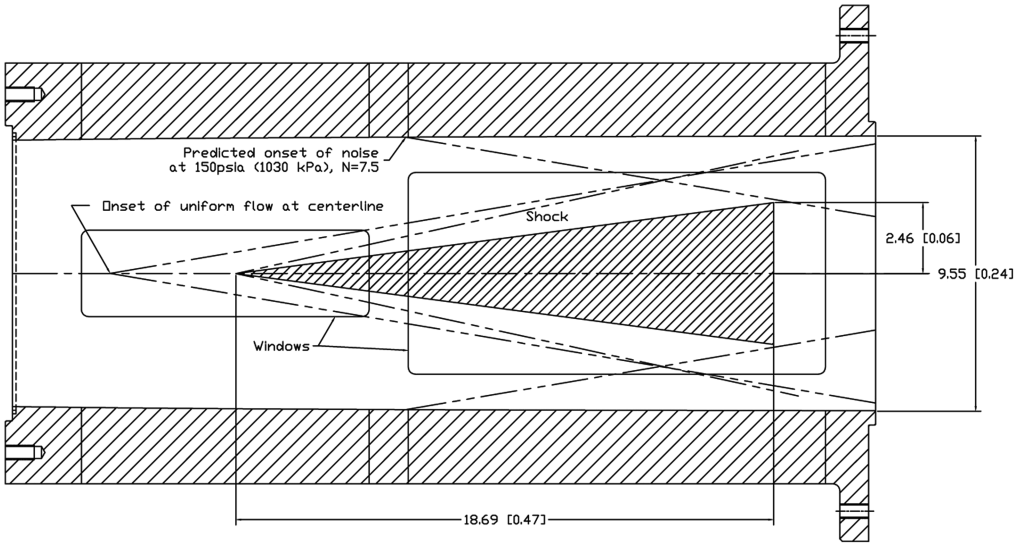

Fig. 2 Schematic of Mach-6 quiet nozzle with 7.5-deg cone model; dimensions are in inches [meters].

openings, all but one of which are presently filled with blank metal inserts.

Operational History of the BAM6QT

The BAM6QT was first run in 2001. Initially, the quiet performance was very disappointing. Though designed to run quietly for stagnation pressures up to 150 psia (1000 kPa), the tunnel was quiet only for $p_t < 8$ psia (55 kPa). Several potential explanations for the low maximum quiet pressure were posed. Their solutions were tested from 2001 to 2005, with no substantial impact on the maximum quiet pressure [9].

In late 2002, a small bump was detected on the lip of the bleed slot near the throat that removes the upstream boundary layer. It was not measured until 2005 for fear of damaging the delicate polish. A surrogate throat was machined from aluminum to the same nominal design as the electroformed throat and tested beginning in February 2005. The surrogate-throat bleed lip did not have the same imperfection. This change was the first to have a significant improvement on the quiet pressure and led to a greater appreciation of the influence of the contour near the bleed lip.

Initial tests with the surrogate yielded maximum quiet pressures of 20 psia (140 kPa). Polishing the surrogate throat and other minor modifications eventually raised the quiet pressure to 90 psia (620 kPa) [14].

In May 2006, the bleed lip of the electroformed nozzle was remachined into an elliptical profile calculated to minimize separation (see the next section). Measurements made before and after the modification confirm the kink and show how it is eliminated (Fig. 3). The two passes were made at azimuthal angles 45 deg apart. The presence of the kink in one pass and not the other indicates that the defect is not axisymmetric. Its precise azimuthal extent is not known, but it was present in two of eight evenly spaced passes, suggesting a size greater than 45 and less than 135 deg [15].

The first tests with the remachined but unpolished electroform were quiet for $p_t < 37$ psia (260 kPa). This nozzle was then repolished and achieved quiet pressures as high as 153 psia (1050 kPa). There were six months of regular operation, up to ten runs per day, five or six days per week, with quiet pressure above 145 psia (1000 kPa) before the performance started to degrade to about 60% of this level [16]. The nozzle has since been repolished and is operating quietly for $p_t < 135$ psia (930 kPa) [17].

Computational Fluid Dynamics Simulations for the Redesign of the Bleed Lip

The experimental study of Klebanoff and Tidstrom [18] showed that the presence of a separation bubble of sufficient size destabilizes the laminar boundary layer downstream of reattachment, thereby leading to an earlier transition to turbulence. It appears that the kink in the electroformed throat exacerbated a natural tendency to form an unstable separation bubble near the lip [19]. Separation bubbles on the bleed lip and associated fluctuations induced near the bleed lip were identified by Schneider et al. [20] as the most likely cause of early transition. Taskinoglu et al. [21,22] were the first to make a detailed computation of separation bubble structure and location. These computations were motivated by earlier computations for the French quiet tunnel [23]. Only the axisymmetric bleed-lip contour has been modeled; the kink discovered on the bleed lip and discussed in the previous section has not been modeled. The objectives of the computational fluid dynamics (CFD) effort are to demonstrate the

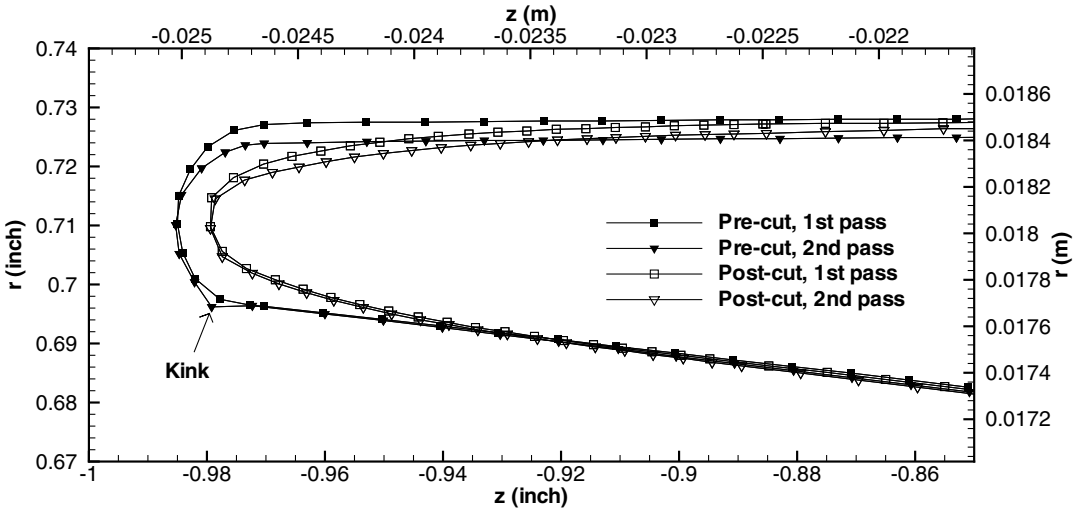

Fig. 3 Precut and postcut measurements of bleed-lip profile by ATK at two different azimuthal locations [15].

effect of separation bubbles on flow structure by numerically investigating the existence of steady and unsteady separation bubbles on the main- or bleed-flow side of the nozzle lip and to design a new geometry to eliminate or reduce the size of the separation bubbles.

Numerical Methodology

Steady and time-accurate computations are performed for both the original geometry and the new designs using GASPex version 4.1.2 [24]. The laminar compressible Navier–Stokes equations are solved. For the modeling of inviscid fluxes, the third-order Roe's scheme with Harten correction is used. The min–mod limiter [25] is employed as a flux limiter to prevent the occurrence of nonphysical oscillations. The boundary conditions are as follows: Po–Riemann subsonic inflow, forced outflow for the bleed-slot and nozzle exits, no-slip adiabatic solid walls, axisymmetric side walls, and an axisymmetric X-axis plane. For the inflow boundary, the total pressure and total density at the boundary are set using Riemann invariants from characteristic theory [24]. The geometry is fully axisymmetric; however, side walls were used for the computational domain, which was a slice of the axisymmetric geometry.

An implicit dual-time-stepping method was used for the time-accurate computations. The time for the flow to go from the bleed lip to the end of the computational domain was calculated to be 0.28 ms. The velocities used for calculating the average velocity are the velocities in the steady-state solution. The total simulation time was taken to be four times the time necessary for the flow to go from the bleed lip to the exit of the computational domain, corresponding to 1.1 ms. The values obtained from the steady-state solution were used for all the flow parameters as an initial condition for the time-accurate computations.

Computational Analysis of the Existing Bleed Slot

Among the modifications made to the tunnel to increase the maximum quiet-flow stagnation pressure, a series of different bleed-slot geometries were tested. The computations were made for the bleed-slot geometry presently installed in the BAM6QT, case 7. This geometry has the best performance of those tested.

Two different grids generated using GridPro/az3000 [26] were used in the computations. The total number of grid points is 99,928 for the first grid. The minimum grid spacing is 0.01 mm around the bleed lip. For the second grid, the minimum grid spacing around the bleed lip is decreased to 0.001 mm and the total number of grid points is 192,184. Grid clustering was performed around the bleed lip with a stretching parameter of 1.105 for both of the grids.

Separation bubbles exist on both the main-flow and the bleed-flow sides of the bleed lip for stagnation pressures of 8, 14, and 150 psia (55, 97, and 1030 kPa) according to steady computational results.

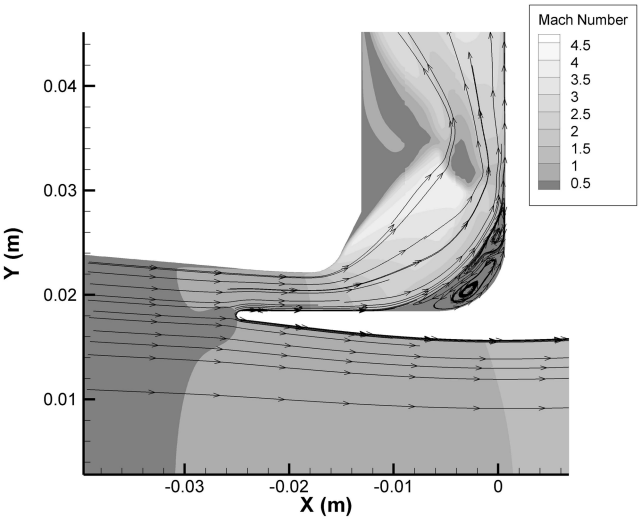

Fig. 4 Mach number contours for case 7.

The lengths of the separation bubbles on the main- and bleed-flow sides of the bleed lip are 1.15 and 2.2 mm, respectively, for the flow at 150 psi (1030 kPa) stagnation pressure. The streamlines superimposed with Mach number contours for the flow at 150 psi (1030 kPa) is shown in Fig. 4. The magnified plot around the bleed lip is shown in Fig. 5.

According to the time-dependent computations, for the flow at 8 psi (55 kPa), no unsteadiness was observed in the flow. Unsteadiness in the flow starts at 14 psi (97 kPa) and continues to exist at higher stagnation pressures. For the flow at 14 psi (97 kPa), unsteadiness was observed in the flow around the separation bubble on the bleed-flow side of the bleed lip only. The wall shear stress values were calculated for the points around the bleed-slot lip.

The shear stress at the wall is defined as

$$\tau_w = \mu_w \frac{\mathbf{s} \cdot \mathbf{V}}{\Delta n} \tag{1}$$

where μ_w is the viscosity, $\mathbf{s}$ is the vector parallel to the surface, $\mathbf{V}$ is the velocity vector, and Δn is distance between the wall and the next grid point. The vector $\mathbf{s}$ is taken as positive in the positive x direction for both the upper and the lower surfaces.

The shear stress variation for the upper surface at 14 psi (97 kPa) for several time values is shown in Figure 6. There is unsteadiness in shear stress at 14 psi (97 kPa). The first location at which the shear stress is negative corresponds to the separation bubble on the bleed-flow side of the lip. The second location at which the shear stress has

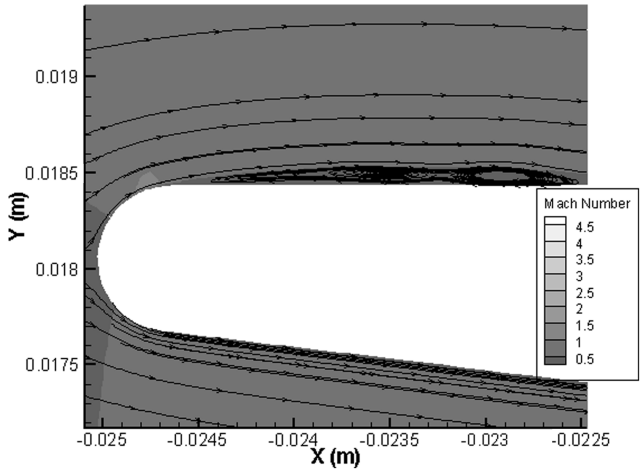

Fig. 5 Streamlines around the bleed slot for case 7 at 150 psi (1030 kPa).

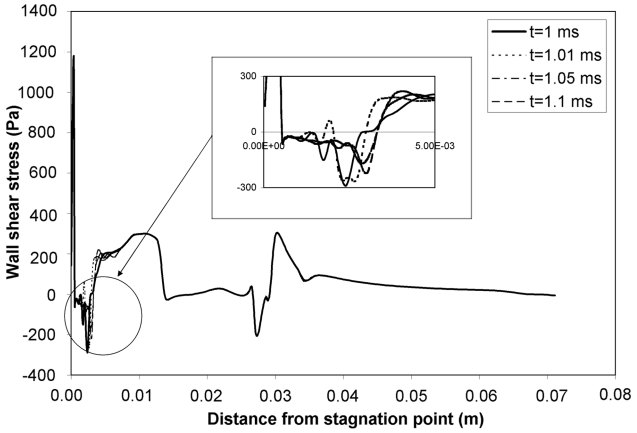

Fig. 6 Shear stress variation for the upper surface at 14 psi (97 kPa).

negative values corresponds to the recirculation region on the corner of the geometry.

Separation bubbles induce earlier transition to turbulent flow by destabilizing the boundary layer, although the presence of a separation bubble (especially on the bleed-flow side) does not guarantee transition. Steady and time-accurate simulation results at several stagnation pressures show that separation bubbles with varying sizes exist on both the main-flow and the bleed-flow sides of the bleed lip of the original electroformed nozzle for all stagnation pressures tested.

Redesign of Bleed Lip

An adverse pressure gradient is present just aft of the blunt nose on a flat plate in uniform flow. As a semi-elliptical nose becomes more slender, this gradient is reduced [27]. The basic idea in the modifications of the bleed lip is to make the lip more slender to eliminate the separation bubbles. Several modifications were made to the case-7 geometry by cutting the bleed lip over an axial region that covers less than 0.1 in. (2.54 mm) [28,29]. The computational results obtained with the most successful geometry will be summarized.

The original and new geometries are shown in Fig. 7. The x coordinate is the axial distance from the throat (negative is upstream). The y coordinate is the radius from the centerline. To obtain the new geometry, the nozzle coordinates after points $(-22.98, 17.48)$ mm were not altered. The coordinates of the upper portion of the bleed lip were not changed after points $(-22.5, 18.45)$ mm. Three arbitrary points were put between these two unaltered original geometry points, and four different cubic splines were fit to these five points to create the new geometry.

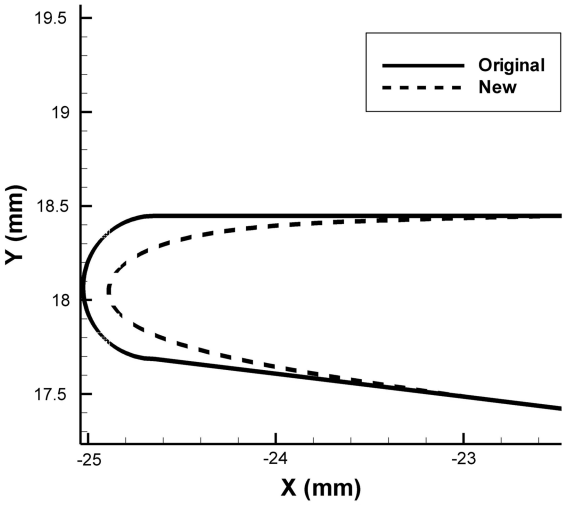

Fig. 7 Original and new geometries.

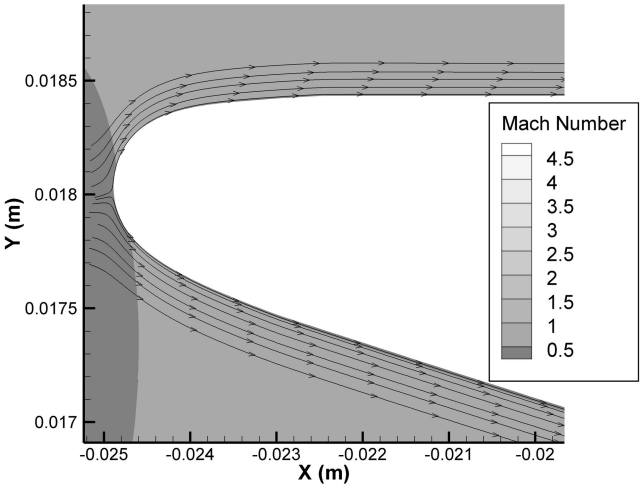

Fig. 8 Mach number contours for the new geometry at 300 psi (2070 kPa).

Steady and unsteady computations were performed on the new geometry for stagnation pressures of 50, 150, and 300 psi (345, 1030, and 2070 kPa) at a stagnation temperature of 433 K. The Mach number contours and streamlines for the steady simulations of the new geometry at 300 psi (2070 kPa) are shown in Fig. 8. The results for 50 and 150 psi (345 and 1030 kPa) stagnation pressure are similar to those at 300 psi (2070 kPa). The separation bubbles on both the lower and upper parts of the bleed lip are eliminated up to a stagnation pressure of 300 psi (2070 kPa).

The wall shear stress plots are shown for the upper and lower sides of the stagnation point at a stagnation pressure of 150 psi (1030 kPa) in Figs. 9 and 10, respectively. There is no unsteadiness in wall shear stress at 150 psi (1030 kPa). The shear stress at the location of the separation bubble that previously existed on the upper side of the bleed lip is high and positive, as seen in Fig. 9.

Steady and unsteady computations with this nozzle lip geometry show that the separation bubbles on both the main- and bleed-flow sides of the nozzle lip are eliminated with this new geometry up to a stagnation pressure of 300 psi (2070 kPa). The separation bubbles that may cause earlier transition in the test section of a hypersonic quiet tunnel can be eliminated by careful design of the geometry of the bleed lip. In the present case, remachining the lip of the nickel throat also eliminated a kink in the original geometry. Thus, there were two ways in which remachining the lip may have affected the flow, and it is not possible to separate the two using existing measurements.

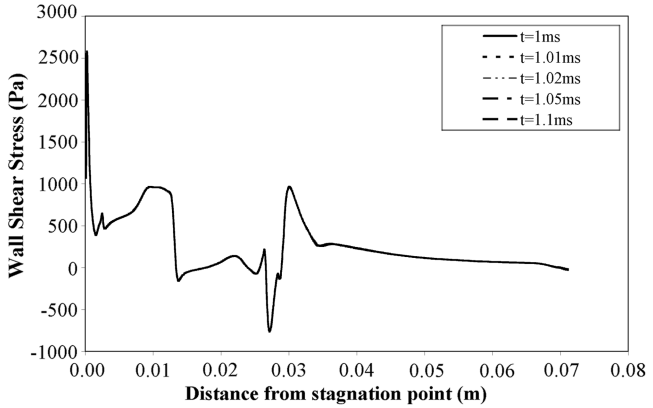

Fig. 9 Shear stress variation for the upper surface of the new geometry at 150 psi (1030 kPa).

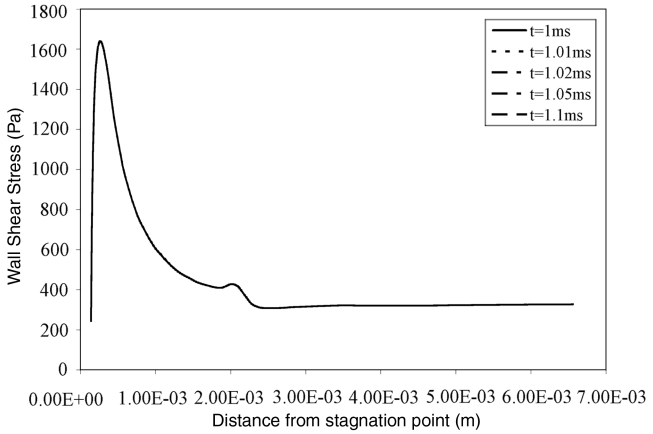

Fig. 10 Shear stress variation for the lower surface of the new geometry at 150 psi (1030 kPa).

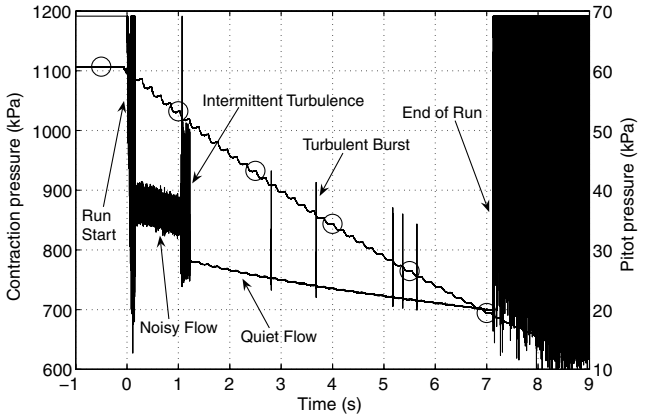

Fig. 11 Pitot pressure showing quiet flow at high pressure (145 psia, 1000 kPa) with few turbulent bursts; there is no model in the tunnel; the sensor is along the centerline 2.37 m downstream of the throat [30].

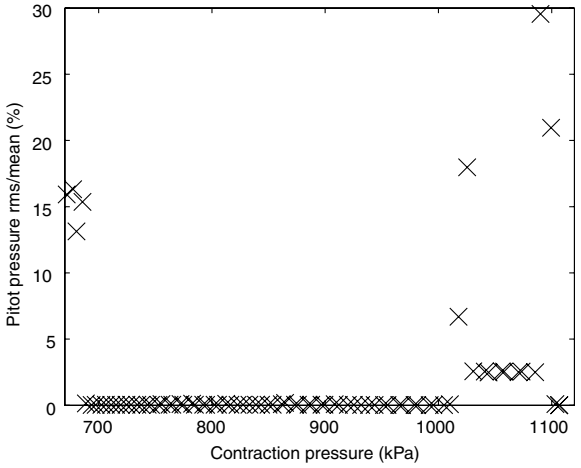

Fig. 12 Typical noise level during a run [30].

Pitot Pressure Data

Figure 11, reproduced from [30], illustrates the substantial difference between noisy and quiet flow. It is a typical oscilloscope trace, with the data converted from voltage to pressure.

High-frequency Kulite pressure transducers (model XCQ-062-15A) are used to measure the pitot pressure. A mechanical stop behind the diaphragm of these transducers allows the test area to be pressurized to the high stagnation pressure without damaging them. The dc pitot pressure is amplified by a factor of 100 before digitization, and the ac pitot pressure is high-pass-filtered at about 840 Hz and amplified by an additional factor of 100 before digitization, using custom-built electronics based on instrumentation-amplifier integrated circuits (INA103). Data were collected on various 8-bit digital oscilloscopes employing an internal high-resolution averaging mode to reduce noise and increase effective resolution from 8 to 11 or 12 bits (Tektronix TDS 7104, 5034, or 7054). Data were recorded for 10 s at 200 kHz. The pressure transducers and associated electronics are calibrated quasi-statically using a quartz pressure transducer (Paroscientific Model 740) by slowly filling the tunnel from vacuum.

The oscilloscope is triggered by the sudden drop in pitot pressure when the diaphragms burst. The first second of data is from before the trigger and provides a baseline of electronic noise. At time $t \simeq 0.0$ s, the diaphragms burst and the run starts. Approximately 0.2 s is required to start up the Mach 6 flow. During this run, the tunnel runs at a conventionally high noise level until $t \simeq 1.0$ s. At $t \simeq 1.0$ s the boundary layer on the nozzle-wall switches from turbulent to intermittently turbulent, becoming laminar and quiet at $t \simeq 1.2$ s. The contraction-wall pressure is highlighted with circles and referred to the left-hand axis. It drops from an initial value of 160 psia (1100 kPa) in stair steps, each time the expansion wave reflects from the contraction. The contraction pressure at which the noise drops to quiet levels is about 146 psia (1000 kPa). With the exception of five turbulent bursts between $t \simeq 2.8$ and 5.7 s, the tunnel is quiet until the run ends at $t \simeq 7.1$ s when the contraction-wall pressure has dropped 28% to about 105 psia (724 kPa). Each turbulent burst has an approximately 1.5-ms duration [14], corresponding to 300 data points per burst. The pressure at which the nozzle drops to quiet has always been essentially independent of the time during the run at which this pressure is achieved.

Noise Level

The pressure data are also used to calculate the tunnel noise level, $\tilde{p}/\bar{p}$. The noise level for the preceding run as a function of contraction pressure is shown in Fig. 12. The noise is computed by breaking the run into 0.1-s intervals and calculating $\tilde{p}$ and $\bar{p}$ over the segment. If the interval is quiet, the high-pass-filtered and amplified ac pitot pressure is used to find $\tilde{p}$; if not, the dc pitot pressure is used.

As expected, the prerun ($p_t > 160$ psia, 1100 kPa) noise level is very small. The noise increases to 2.4 to 2.6% until $p_t = 149$ psia (1030 kPa), at which point the noise increases to near 18% during the series of turbulent bursts. When $p_t < 146$ psia (1010 kPa), the noise level decreases below 0.05%, except for the occasional turbulent spot (Fig. 13). The noise level increases dramatically when the run ends ($p_t < 100$ psia, 690 kPa).

The modifications made to the tunnel did not change the basic pattern of pitot pressure vs time or the noise level vs contraction

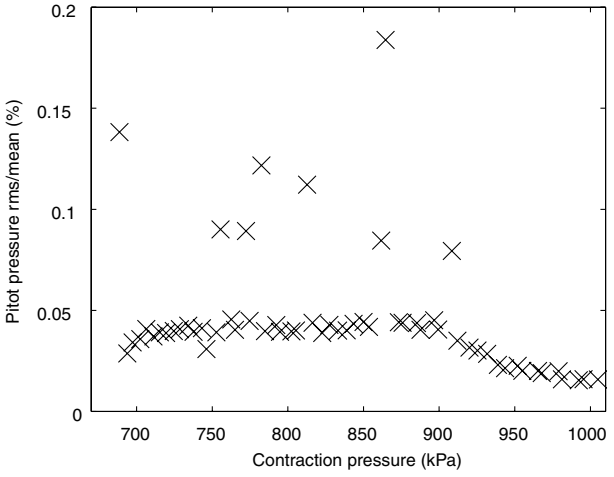

Fig. 13 Typical noise level during the quiet portion of a run [30].

pressure. Rather, the goal was to increase the contraction pressure at which the changeover from noisy to quiet flow occurred. Thus, after most runs, data analysis consisted of applying the transducer calibrations to the oscilloscope data and identifying the maximum quiet pressure for that run. The reduction in noise level at the onset of quiet flow is quite pronounced and easily ascertained.

Conclusions

The BAM6QT has achieved its target of quiet operation for a unit Reynolds number of 3.4×10^6/ft (11×10^6/m). Several substantial restrictions on performance were identified and overcome. As originally fabricated, the electroformed nozzle was limited to a maximum quiet pressure of 8 psia (55 kPa) by the small kink near the tip on the main-flow side of the bleed lip. Testing of an aluminum surrogate nozzle with the original hemispherical bleed-lip profile but without the flaw yielded quiet pressures up to 90 psia (620 kPa). Finally, machining the nickel throat to the elliptical profile provided by the CFD calculations enabled maximum quiet pressures as high as 153 psia (1050 kPa). Both the electroformed nickel and surrogate nozzles demonstrated performance improvements as a result of polishing surfaces that had previously had a rougher finish. The BAM6QT is currently the only operational hypersonic tunnel providing high-Reynolds-number quiet flow with low noise levels that are comparable with those in flight.

Acknowledgments

The research is funded by the U.S. Air Force Office of Scientific Research under grants FA9550-06-1-0182 and FA9550-05-1-0014, by Sandia National Laboratory under grant PR858548, by NASA Johnson Space Center under grant NNJ06HD32G, by NASA Langley Research Center under grant 102361, and by the NASA Constellation University Institutes Project program. All computations were performed at the Rutgers University computational cluster. The delicate and critical remachining of the nickel bleed lip was capably performed by ATK/Microcraft of Tullahoma, Tennessee.

References

[1] Schneider, Steven P.. "Laminar–Turbulent Transition on Reentry Capsules and Planetary Probes," *Journal of Spacecraft and Rockets*, Vol. 43, No. 6, Nov.–Dec. 2006, pp. 1153–1173. doi:10.2514/1.22594

[2] Schneider, Steven P.. "Hypersonic laminar–turbulent Transition on Circular Cones and Scramjet Forebodies," *Progress in Aerospace Sciences*, Vol. 40, No. 1–2, Feb. 2004, pp. 1–50. doi:10.1016/j.paerosci.2003.11.001

[3] Beckwith, I. E., and Miller, C. G., III., "Aerothermodynamics and Transition in High-Speed Wind Tunnels at NASA Langley," *Annual Review of Fluid Mechanics*, Vol. 22, 1990, pp. 419–439. doi:10.1146/annurev.fl.22.010190.002223

[4] Schneider, Steven P.. "Effects of High-Speed Tunnel Noise on Laminar–Turbulent Transition," *Journal of Spacecraft and Rockets*, Vol. 38, No. 3, May–June 2001, pp. 323–333.

[5] Schneider, Steven P.. "Flight Data for Boundary-Layer Transition at Hypersonic and Supersonic Speeds," *Journal of Spacecraft and Rockets*, Vol. 36, No. 1, Jan.–Feb. 1999, pp.8–20.

[6] Wilkinson, S. P., Anders, S. G., and Chen, F.-J, "Status of Langley Quiet Flow Facility Developments," AIAA, Paper 94-2498, June 1994.

[7] Beckwith, I., Creel, T., Chen, F., and Kendall, J., "Freestream Noise and Transition Measurements on a Cone in a Mach-3.5 Pilot Low-Disturbance Tunnel," NASA, TP 2180, Sept. 1983.

[8] Blanchard, A. E., Lachowicz, J. T., and Wilkinson, S. P., "NASA Langley Mach 6 Quiet Wind-Tunnel Performance," *AIAA Journal*, Vol. 35, No. 1, Jan. 1997, pp. 23–28.

[9] Schneider, S. P., "The Development of Hypersonic Quiet Tunnels," AIAA Paper 2007-4486, June 2007.

[10] Beckwith, I. E., Harvey, W. D., Harris, J. E., and Holley, B. B., "Control of Supersonic Wind-Tunnel Noise by Laminarization of Nozzle-Wall Boundary Layers," NASA Langley Research Center, TM X-2879, Hampton, VA, Dec. 1973, p. 23665.

[11] Harvey, W. D., Stainback, P. C., Anders, J. B., and Cary, A. M., "Nozzle Wall Boundary-Layer Transition and Freestream Disturbances at Mach 5," *AIAA Journal*, Vol. 13, No. 3, Mar. 1975, pp. 307–314.

[12] Schneider, Steven P., "Design and Fabrication of a 9.5-Inch Mach-6 Quiet-Flow Ludwieg Tube," AIAA Paper 1998-2511, June 1998.

[13] Carmichael, B. H., "Summary of Past Experience in Natural Laminar Flow and Experimental Program for Resilient Leading Edge," NASA, CR 152276, May 1979.

[14] Juliano, Thomas J., "Nozzle Modifications for High-Reynolds-Number Quiet Flow in the Boeing/AFOSR Mach-6 Quiet Tunnel," M.S. Thesis, School of Aeronautics and Astronautics, Purdue Univ., West Lafayette, IN, Dec. 2006; also Defense Technical Information Center, Rept. ADA456772, Ft. Belvoir, VA, Dec. 2006.

[15] Schneider, S. P., Juliano, T. J., and Borg, M. P., "High-Reynolds-Number Laminar Flow in the Mach-6 Quiet-Flow Ludwieg Tube," AIAA Paper 2006-3056, June 2006.

[16] Schneider, S. P., and Juliano, T. J., "Laminar–Turbulent Transition Measurements in the Boeing/AFOSR Mach-6 Quiet Tunnel," AIAA Paper 2007-4489, June 2007.

[17] Borg, M. P., Schneider, S. P., and Juliano, T. J., "Effect of Freestream Noise on Roughness-Induced Transition for the X-51A Forebody," AIAA Paper 2008-0592, Jan. 2008.

[18] Klebanoff, P. S., and Tidstrom, K. D., "Mechanism by Which a Two-Dimensional Roughness Element Induces Boundary-Layer Transition," *Physics of Fluids*, Vol. 15, No. 7, July 1972, pp. 1173–1188. doi:10.1063/1.1694065

[19] Haggmark, C. P., Hildings, C., and Henningson, D. S., "A Numerical and Experimental Study of a Transitional Separation Bubble," *Aerospace Science and Technology*, Vol. 5, No. 5, July 2001, pp. 317–328. doi:10.1016/S1270-9638(01)01110-5

[20] Schneider, S. P., Matsumura, S., Rufer, S., Skoch, C., and Swanson, E., "Hypersonic Stability and Transition Experiments on Blunt Cones and a Generic Scramjet Forebody," AIAA Paper 2003-1130, Jan. 2003.

[21] Taskinoglu, E. S., Knight, D. D., and Schneider, S. P., "A Numerical Analysis of the Bleed Slot Design of the Purdue Mach-6 Wind Tunnel," AIAA Paper 2005-0901, Jan. 2005.

[22] Taskinoglu, E. S., Knight, D. D., and Schneider, S. P., "Computational Fluid Dynamics Evaluation of Bleed Slot of Purdue Mach 6 Quiet Tunnel," *AIAA Journal*, Vol. 44, No. 6, June 2006, pp. 1360–1362.

[23] Benay, R., and Chanetz, B., "Design of a Boundary Layer Suction Device for a Supersonic Quiet Wind Tunnel by Numerical Simulation," *Aerospace Science and Technology*, Vol. 8, No. 4, Apr. 2004, pp. 255–271. doi:10.1016/j.ast.2003.11.003

[24] GASPex, Software Package, Ver. 4.1.2, Aerosoft, Inc., Blacksburg, VA, 2004.

[25] Tannehill, J. C., Anderson, D. A., and Pletcher, R. H., *Computational Fluid Mechanics and Heat Transfer*, Taylor and Francis, Levittown, PA, 1984, p. 209.

[26] GridPro/az3000, Software Package, Ver. 4.2.1, Program Development Corp., White Plains, NY, 1998.

[27] Hess, J. L., and Smith, A. M. O., "Calculation of Potential Flow About Arbitrary Bodies," *Progress in Aeronautical Sciences*, Vol. 8, 1967, pp. 1–138. doi:10.1016/0376-0421(67)90003-6

[28] Aradag, S., Knight, D. D., and Schneider, S. P., "Computational Design of the Boeing/AFOSR Mach 6 Wind Tunnel," AIAA Paper 2006-1434, Jan. 2006.

[29] Aradag, S., Knight, D. D., and Schneider, S. P., "Bleed Lip Geometry Effects on the Flow in a Hypersonic Wind Tunnel," *AIAA Journal*, Vol. 44, No. 9, Sept. 2006, pp. 2133–2136. doi:10.2514/1.23064

[30] Juliano, T. J., Swanson, E. O., and Schneider, S. P., "Transition Research and Improved Performance in the Boeing/AFOSR Mach-6 Quiet Tunnel,". AIAA Paper 2007-0535, Jan. 2007.

R. Lucht
Associate Editor